# Optimization of Perturbed Spacecraft Trajectories Using Complex Dual Numbers. Part 2: Numerical Results

## V. G. Petukhov[a], * and Sung Wook Yoon[b], **

*[a] Research Institute of Applied Mechanics and Electrodynamics, Moscow Aviation Institute, Moscow, Russia*
*[b] Moscow Aviation Institute, Moscow, Russia*
*\*e-mail: vgpetukhov@gmail.com*
*\*\*e-mail: wook4573@naver.com*

**Abstract**—Numerical results are presented for optimizing the perturbed trajectories of spacecraft with finite-thrust. The optimal trajectories are calculated using an indirect approach based on the application of the necessary optimality conditions in the form of the maximum principle, the method of continuation by parameter, and complex dual numbers for high-precision calculation of the necessary derivatives of complicated functions. This approach was presented in the first part of the paper. The aim of optimization problem is to calculate trajectories with minimal fuel consumption for a given angular distance and free transfer duration. A mathematical model of the spacecraft motion in equinoctial elements with an angular independent variable is used. Typical examples of optimal perturbed multi-revolution trajectories between high elliptical orbits, between geostationary transfer orbit and geostationary orbit, and between near-circular low Earth orbits are considered. A comparison is made between the optimal perturbed and unperturbed trajectories. The estimation of the influence of the departure date, the angular distance of the transfer and the set of the perturbing accelerations on the main parameters of the optimal trajectories is given.

**Keywords:** optimal multi-revolution transfers, perturbed trajectories, maximum principle, continuation method, complex dual numbers

**DOI:** 10.1134/S0010952521060083

## INTRODUCTION

The first part of the article [1] contains a detailed description of a new method for optimizing perturbed finite-thrust spacecraft trajectories based on the application of the maximum principle, the continuation method, and the algebra of complex dual numbers for high-precision calculation of the required derivatives. In this article, we present numerical results of the optimization of trajectories between various Earth orbits using this method.

To illustrate the capabilities of the method, we consider perturbing accelerations from the geopotential harmonics up to the fourth order and fourth degree inclusive and the lunisolar perturbations. This set of perturbations is considered for all the problems, unless another model of perturbing accelerations is specifically indicated. The EGM-96 model [2] was used as a mathematical model of the Earth's gravitational field. The precession and nutation matrices were fixed at the initial time point, and the matrix of the proper motion of the pole was taken to be unity. The ephemerides of the Moon and the Sun were calculated using the DE405 data [3]. The gravitational parameter of the Sun was taken equal to

$0.13712440017987 \times 10^{21}$ m$^3$/s$^2$ and the gravitational parameter of the Moon as $0.4902799 \times 10^{13}$ m$^3$/s$^2$.

The determining factor for different orbit transfers is the different set of major perturbing accelerations. Obviously, for transfers between very high orbits with an apogee radius comparable to the radius of the Moon's orbit, the lunisolar perturbations should be considered as major perturbing accelerations that determine the main parameters of the trajectory. For typical transfers of spacecraft with an electric propulsion system (EPS) to a geostationary orbit (GEO), the influence of the nonspherical Earth's gravitational potential and the lunisolar perturbations is significant. Lastly, transfers between low Earth orbits are most significantly affected by the nonspherical Earth's gravitational field. In this regard, the first section of this paper presents the results of optimization between high elliptical orbits; the second section, the results of optimization of multi-revolution trajectories between the geostationary transfer orbit and the GEO; and the third section, the results of optimization of a multi-revolution transfer between near-circular low Earth orbits. For the transfers considered in the second and third chapters, there are a number of numerical results

obtained by other authors; these examples were used to assess the reliability of the results obtained with the method from [1]. The article presents the numerical results of solving boundary-value problems of the maximum principle for perturbed and unperturbed trajectories and analyzes the effect of the initial time of the transfer, the angular distance of the transfer, and the set of the perturbing accelerations on the parameters of optimal perturbed trajectories.

## 1. OPTIMIZATION OF THE TRANSFER TRAJECTORY BETWEEN TWO ELLIPTICAL ORBITS

The first problem that we consider is the problem of optimizing fuel consumption for a transfer of a spacecraft with an EPS between initial and final elliptical orbits the parameters of which are presented in Table 1. The fixed angular distance of transfer is 5 revolutions. The heights of the perigee and apogee of the initial and final orbits hereinafter are given relative to the mean radius of the Earth (6371 km).

The initial mass of the spacecraft is taken equal to 1000 kg, the EPS thrust is 0.5 N, and the specific impulse is 1520 s. The numerical results of solving optimal control boundary-value problem (8)–(10) from [1] for the given initial data and the initial transfer date of May 9, 2021, 12:00 UTC for the trajectory with the listed perturbations and the unperturbed trajectory are given in Table 2; the relative errors in the orbital elements for these trajectories are given in Table 3.

Figure 1 shows the projections of the optimal unperturbed and perturbed trajectories onto the coordinate planes. Segments of the trajectory with operating EPS are indicated by thick solid lines, coasting segments of the unperturbed trajectory by thin solid lines, and coasting segments of the perturbed trajectory by dashed lines. It can be seen from the figure that the action of the perturbing accelerations leads to a significant deformation of the optimal trajectory. The qualitative difference of the perturbed trajectory in the case under consideration is the absence of a segment with operating EPS at the beginning of the transfer.

Figure 2 shows the time dependences of the orbital elements in unperturbed and perturbed optimal trajectories. The dependences for the unperturbed trajectory are represented by solid lines, and for the perturbed trajectory by dashed lines. The time dependences of the switching function, pitch angle, and yaw angle in the optimal unperturbed (solid lines) and perturbed (dashed lines) trajectories are shown in Fig. 3. A large difference is seen between the time dependences of the yaw angle for the perturbed and unperturbed trajectories.

Figure 4 shows the dependences of the final spacecraft mass and the optimal transfer duration on the departure date for the optimal unperturbed (dashed line) and perturbed (solid line) trajectories. To con-

**Table 1.** Initial and final orbit parameters

|  | Initial orbit | Final orbit |
|---|---|---|
| Perigee altitude, km | 500 | 20 000 |
| Apogee altitude, km | 600 000 | 250 000 |
| Inclination, deg | 50 | 65 |
| Right ascension of the ascending node, deg | 0 | 320 |
| Argument of perigee, deg | 100 | 90 |
| True longitude, deg | 160 | 1960 |

**Table 2.** Initial values of dimensionless costate variables for perturbed and unperturbed optimal transfer trajectories between elliptical orbits

|  | Perturbed trajectory | Unperturbed trajectory |
|---|---|---|
| $p_p$ | 0.097657723 | 0.174121297 |
| $p_{ex}$ | 0.009133118 | −0.027603781 |
| $p_{ey}$ | 0.067734445 | 0.239003689 |
| $p_{ix}$ | 0.050282471 | 0.013836165 |
| $p_{iy}$ | 0.020409383 | 0.003738602 |
| $p_{Lk}$ | $1.533357887 \times 10^{-5}$ | $-6.498740712 \times 10^{-6}$ |
| $p_t$ | $1.788597491 \times 10^{-5}$ | $1.962669196 \times 10^{-24}$ |
| $p_m$ | −0.056255821 | −0.057428138 |
| $K_f$, deg | 1817.367048750 | 1818.033626880 |
| $m_f$, kg | 956.069829275 | 955.257737953 |
| $\Delta t$, days | 60.453857879 | 60.669362453 |

**Table 3.** Relative errors in finite values of orbital elements for optimal perturbed and unperturbed transfer trajectories between elliptical orbits

| Relative errors | Perturbed trajectory | Unperturbed trajectory |
|---|---|---|
| $p$ | $8.546 \times 10^{-5}$ | $-7.718 \times 10^{-6}$ |
| $e$ | $3.595 \times 10^{-5}$ | $-3.231 \times 10^{-6}$ |
| $i$ | $-1.775 \times 10^{-6}$ | $8.861 \times 10^{-9}$ |
| $\Omega$ | $9.090 \times 10^{-7}$ | $1.037 \times 10^{-8}$ |
| $\omega$ | $5.976 \times 10^{-5}$ | $-5.383 \times 10^{-6}$ |
| $L$ | $9.796 \times 10^{-11}$ | $-5.102 \times 10^{-13}$ |

struct these dependences, the optimal perturbed trajectories were calculated with departure times in the range from May 1, 2021, 12:00 UTC to May 31, 2021, 12:00 UTC with a step of 1 day. The values of the final mass and the optimal transfer duration on the unperturbed trajectory are represented by a dashed line. It can be seen from Fig. 4 that, in this case, perturbations almost always allow for an increase in the mass of the spacecraft delivered to the final orbit. The maximum mass increase (by 5.91 kg) is achieved if the transfer is
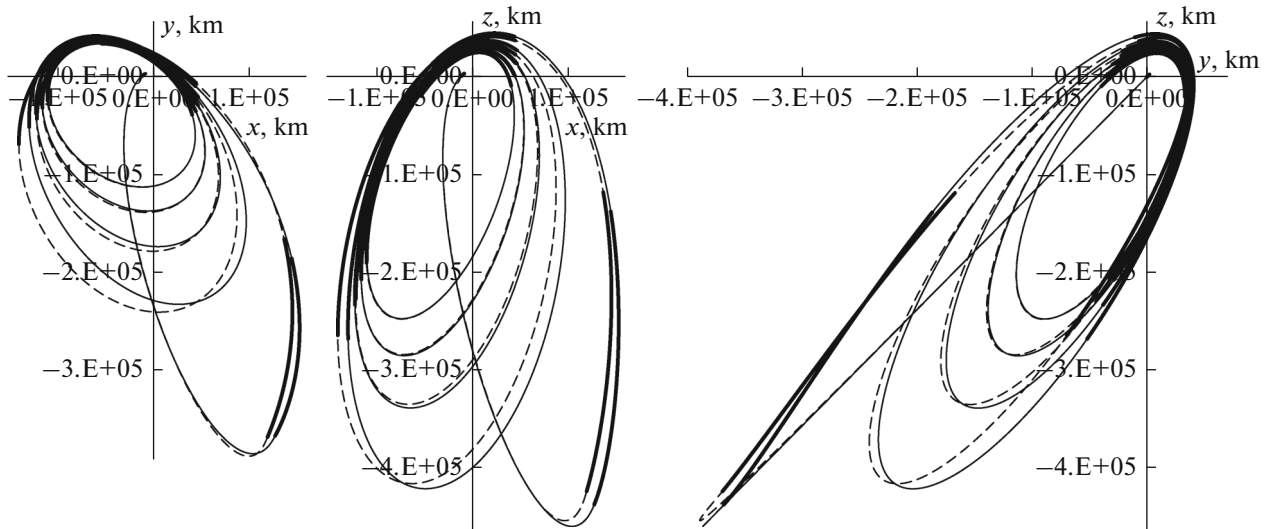
**Fig. 1.** Projections of the optimal unperturbed and perturbed trajectories onto the coordinate planes.
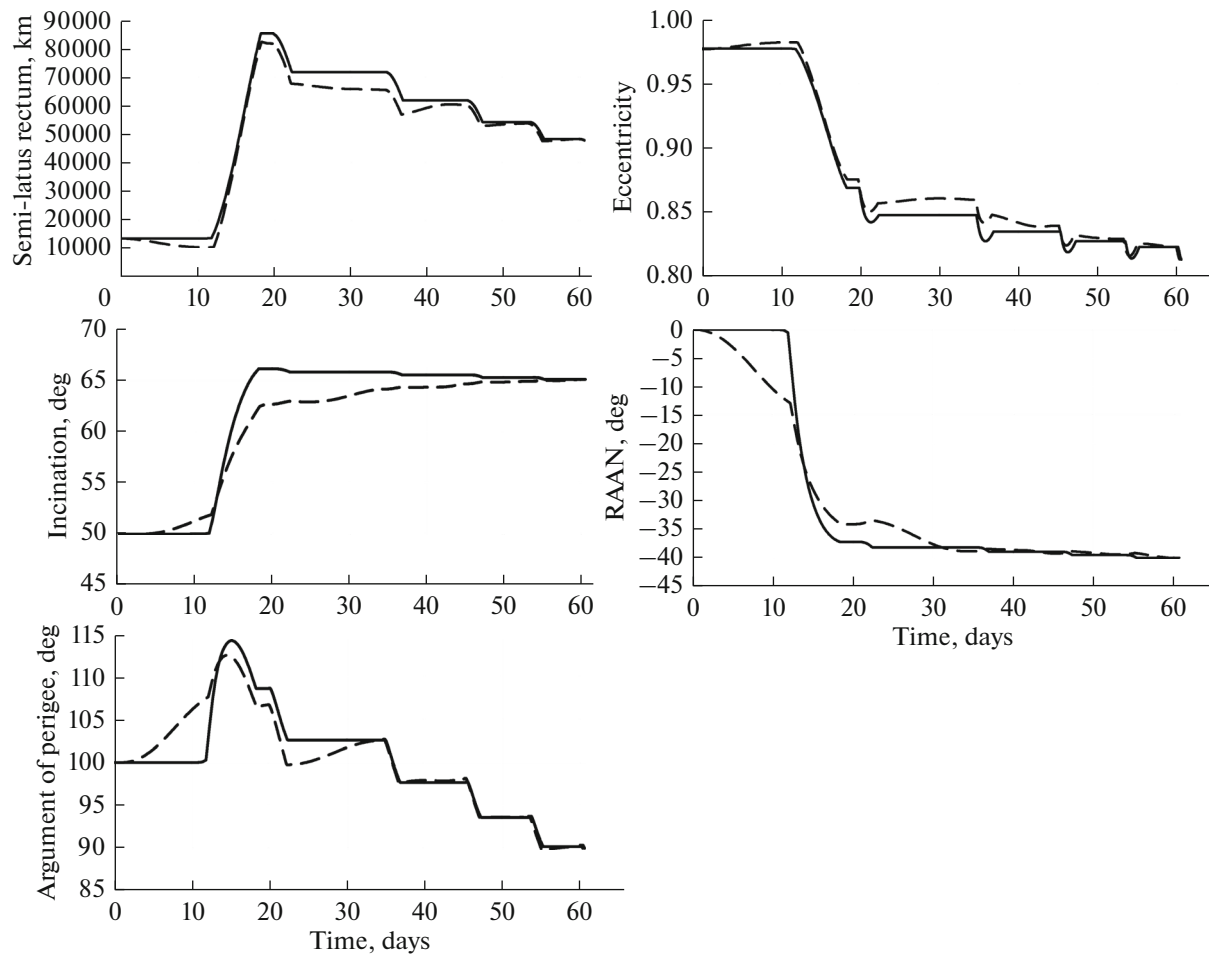


**Fig. 2.** Time dependences of the orbital elements for the optimal unperturbed and perturbed trajectories.
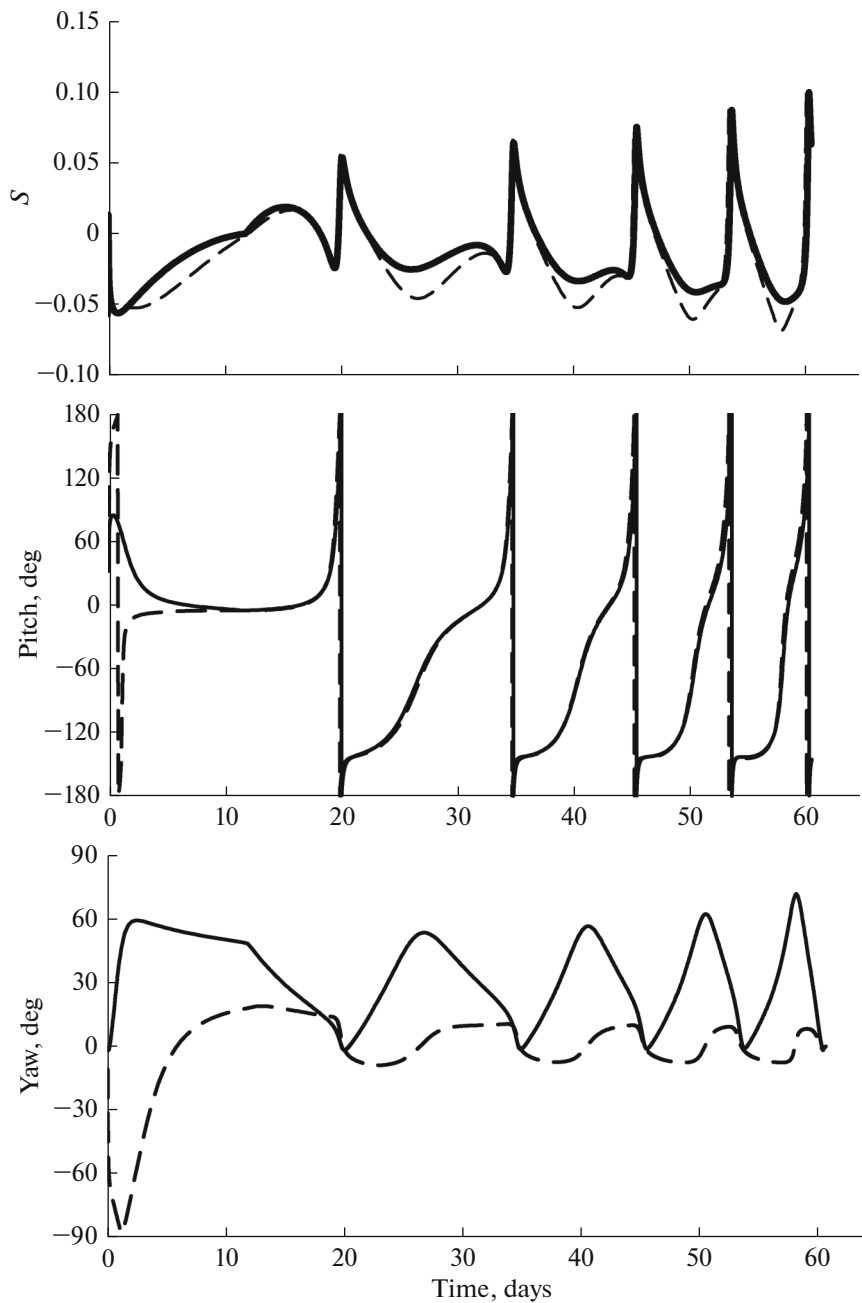
**Fig. 3.** Time dependence of the switching function (top), pitch angle (middle), and yaw angle (bottom) for the optimal unperturbed and perturbed trajectories.

started on May 13, 2021. The only date for the start of the transfer at which the acting perturbing accelerations lead to a decrease in the final mass of the spacecraft (by 0.68 kg) was May 21, 2021. On average, the perturbing accelerations in May 2021 make it possible to increase the mass of the spacecraft delivered to the final orbit by 1.5 kg. The optimal transfer duration for the perturbed trajectory is, on average, 0.92 days less than for the unperturbed trajectory. However, due to the action of perturbations on certain initial dates of the transfer, the optimal duration of the perturbed trajec-

tory can be 2.34 days longer (departure date of May 25) or 3.74 days shorter (departure date of May 12) than the unperturbed trajectory.

Figure 5 illustrates the dependences of the dimensionless initial values of the costate variables for the optimal perturbed trajectories on the departure date. The complicated nature of these dependences is determined, first of all, due to the strong influence of the lunar gravitational perturbing accelerations in the considered interval of the departure dates, during which
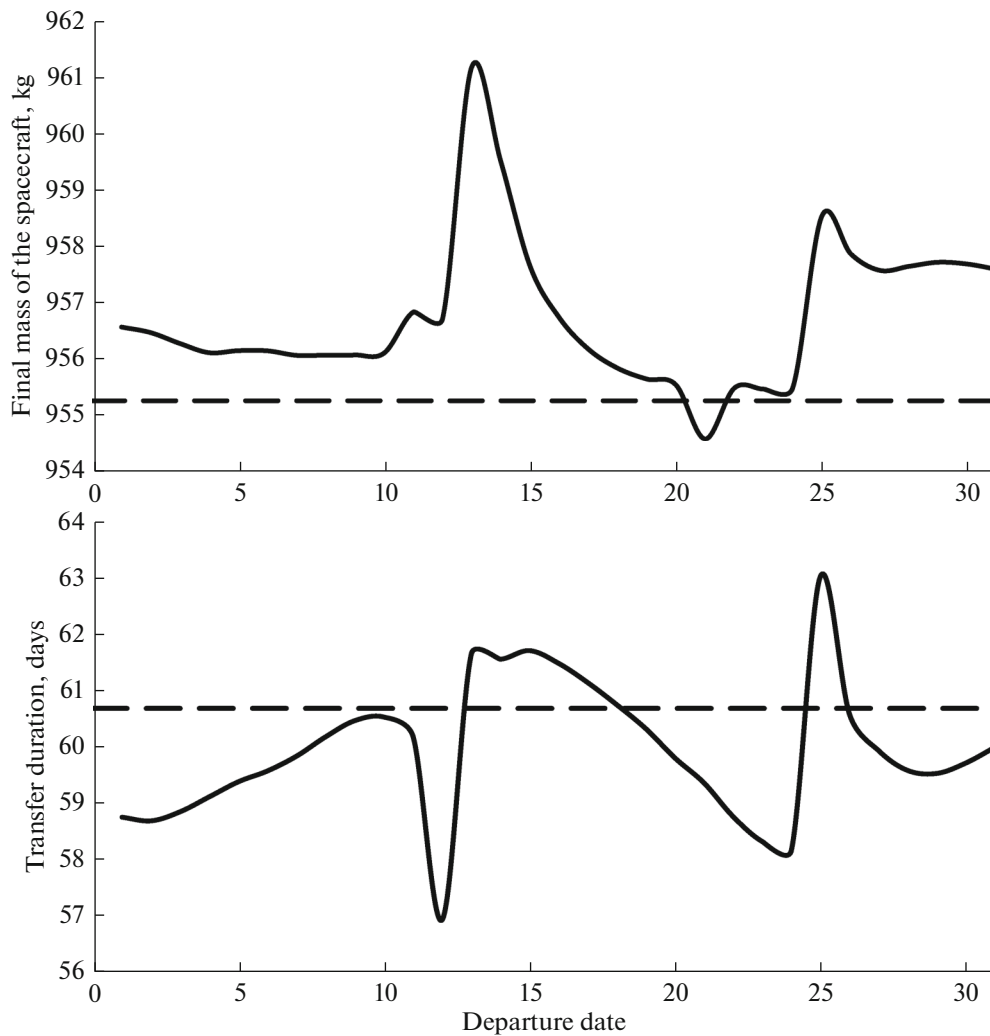
**Fig. 4.** Dependences of the final spacecraft mass (top) and the optimal transfer duration (bottom) on the departure date for the optimal unperturbed (dashed line) and perturbed (solid line) trajectories.

the Moon makes more than one revolution around the Earth.

## 2. OPTIMIZATION OF THE TRANSFER TRAJECTORY BETWEEN GEOSTATIONARY TRANSFER AND GEOSTATIONARY ORBITS

As a second example, let us consider the transfer of a spacecraft with an EPS from an initial (geostationary transfer) orbit with a semimajor axis of 24505.9 km, eccentricity of 0.725, inclination of 7°, zero values of the argument of perigee, and right ascension of the ascending node to the final circular equatorial orbit with a radius of 42 165 km (geostationary orbit). The initial value of the true anomaly is taken to be 0; the initial date of the transfer is January 1, 2000, 12:00:00 UTC; the initial spacecraft mass is 2000 kg; the EPS thrust is 0.35 N; the EPS specific impulse is 2000 s; and the angular distance of transfer is between 200 to 500 revolutions.

The problem corresponds to case B from [4−6]. The results in [4, 5] were presented only for the averaged problem. The solution of the non-averaged unperturbed and perturbed problems is given in [6]. In the case of the perturbed problem in [6], only accelerations from the second zonal harmonic of the geopotential and the lunar gravity perturbation were taken into account, and the problem was solved using differential dynamic programming and the Sundman transformation to the generalized true, mean, or eccentric anomaly.

In [6], the values of fuel consumption $m_p$ and transfer duration $\Delta t$ are presented for 500-revolutions trajectories depending on the set of perturbations and the independent variable used in the mathematical model of spacecraft motion (true or eccentric anomaly): $m_p = 152.77$ kg, $\Delta t = 318.55$ days for the unperturbed trajectory and $m_p = 157.93$ kg, $\Delta t = 320.08$ days for the perturbed trajectory taking into account perturbations
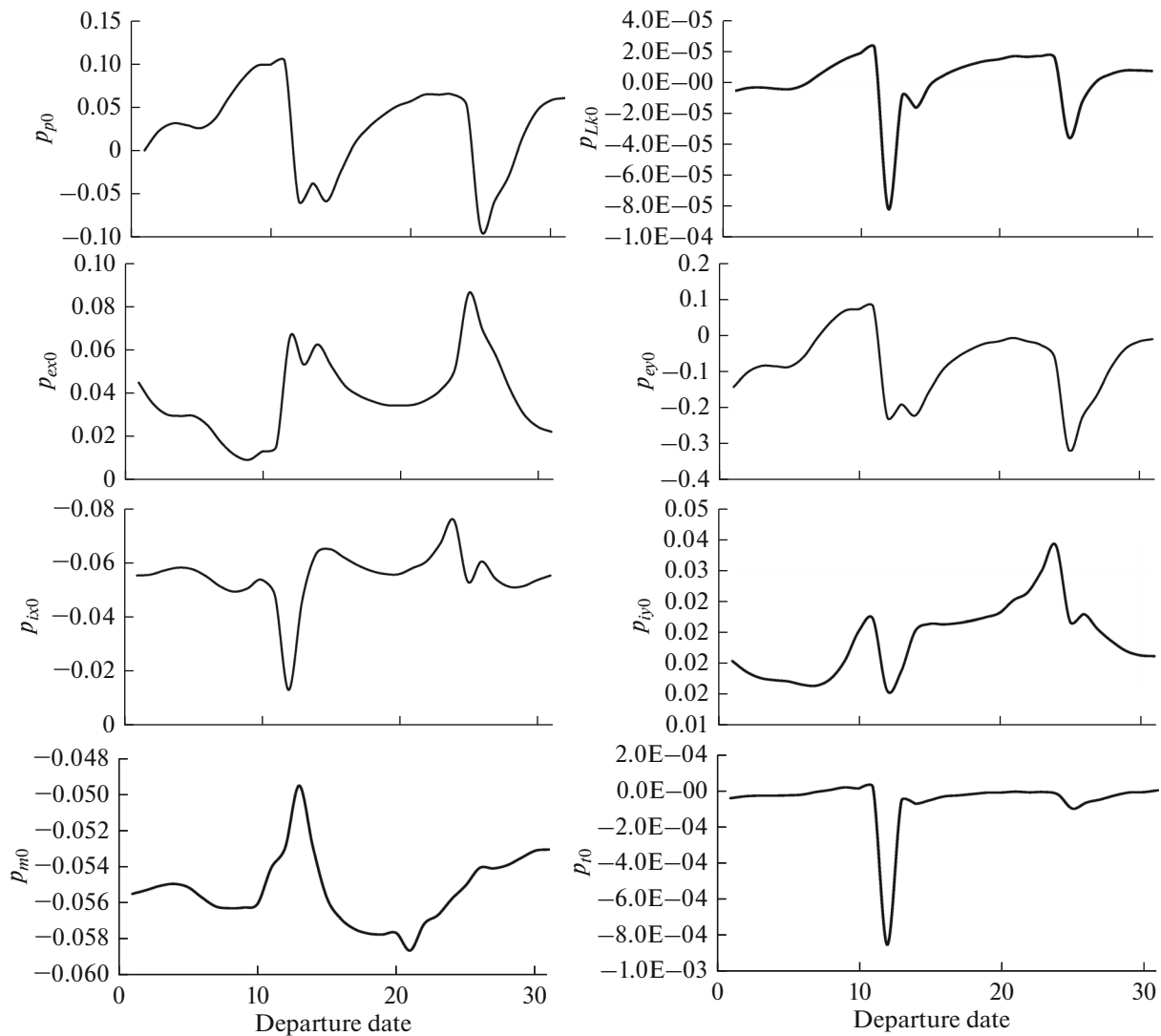
**Fig. 5.** Dependence of the initial values of the costate variables on the departure date for the optimal perturbed trajectories.

from the second zonal harmonic of the geopotential $J_2$ and the lunar gravity perturbation when the true anomaly is used as an independent variable. Using the method based on the use of complex dual numbers, we obtained the following results: $m_p = 152.46$ kg, $\Delta t = 318.88$ days for the unperturbed trajectory and $m_p = 156.87$ kg, $\Delta t = 321.05$ days for the perturbed trajectory taking into account perturbations from the terms of the expansion of the geopotential up to the fourth order and the fourth degree inclusive, as well as the lunisolar gravity.

The optimal transfer duration obtained in our study slightly exceeds the duration of the optimal transfer options given in [6], while the resulting fuel consumption, on the contrary, is less. From comparison of the results, we can conclude that the unperturbed and perturbed trajectories obtained in [6] and in our study are close. The small difference between the results for the

perturbed trajectories in [6] and in this study can be explained by the difference in the set of perturbations (we consider not only $J_2$, but the full $4 \times 4$ matrix of the geopotential and, additionally, lunar gravity). The difference in the fuel consumption for the unperturbed trajectories is 0.20%, and the difference in the transfer duration is 0.10%.

Figure 6 shows the projections onto the coordinate planes of the J2000 coordinate system and the spatial view of the unperturbed and perturbed optimal 500-revolution trajectories (the black solid line indicates trajectory segments with operating EPS, and the gray solid line indicates coasting trajectory segments). Figure 7 illustrates the time dependences of the right ascension of the ascending node, the argument of perigee, and inclination for the optimal unperturbed and perturbed trajectories presented in Fig. 6. One can see a large difference between these dependences for the
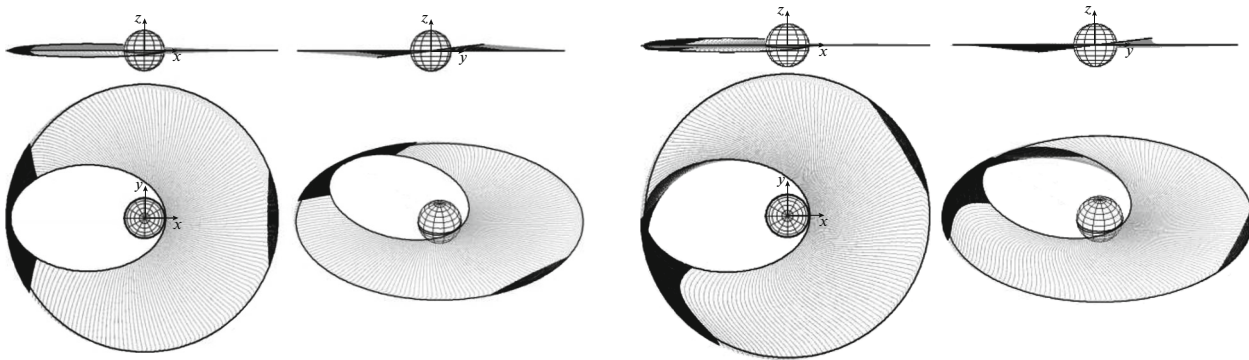
**Fig. 6.** Projections onto the coordinate planes of the J2000 coordinate system and the spatial view of the unperturbed (left) and perturbed (right) optimal 500-revolutions trajectories.
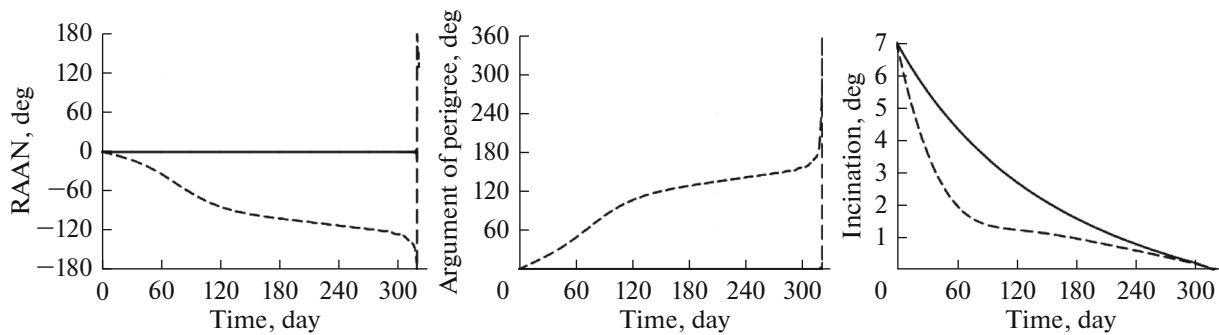


**Fig. 7.** Time dependences of the right ascension of the ascending node (left), argument of perigee (middle), and inclination (right) for the unperturbed (solid lines) and perturbed (dashed lines) 500-revolutions trajectories.
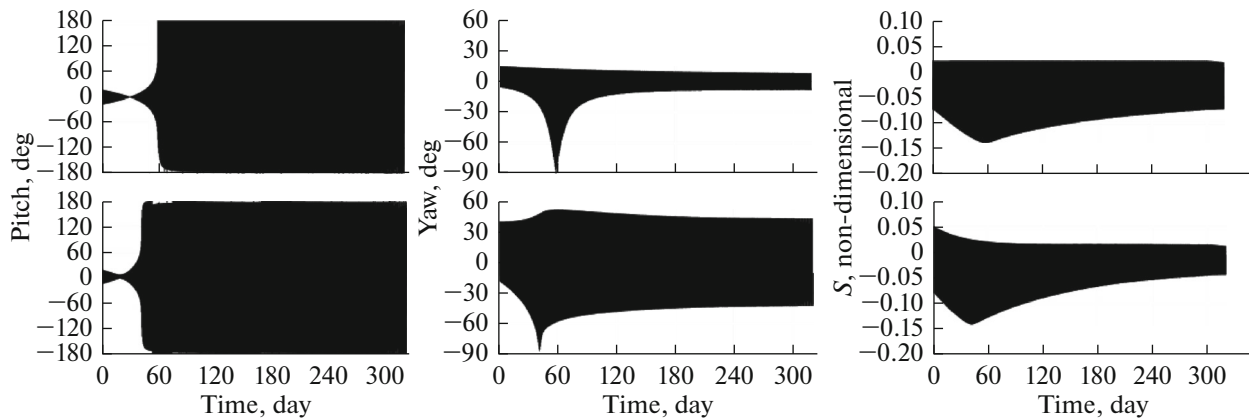


**Fig. 8.** Time dependences of the pitch angle (left), yaw angle (middle), and switching function $S$ (right) for the unperturbed (top row) and perturbed (bottom row) 500-revolutions trajectories.

unperturbed and perturbed trajectories, while the time dependences of the eccentricity and semimajor axis for the unperturbed and perturbed trajectories turned out to be close. Figure 8 presents the time dependences of the pitch angle, yaw angle, and switching function $S$ for an unperturbed and perturbed 500-revolutions trajectories. A significant difference can be

seen in the optimal yaw program and the time dependence of the switching function.

Figure 9 shows the projections of the perturbed optimal trajectory with 200–350 revolutions onto the equatorial plane taking into account perturbations from the harmonics of the geopotential to the fourth degree and fourth order, inclusive, as well as the
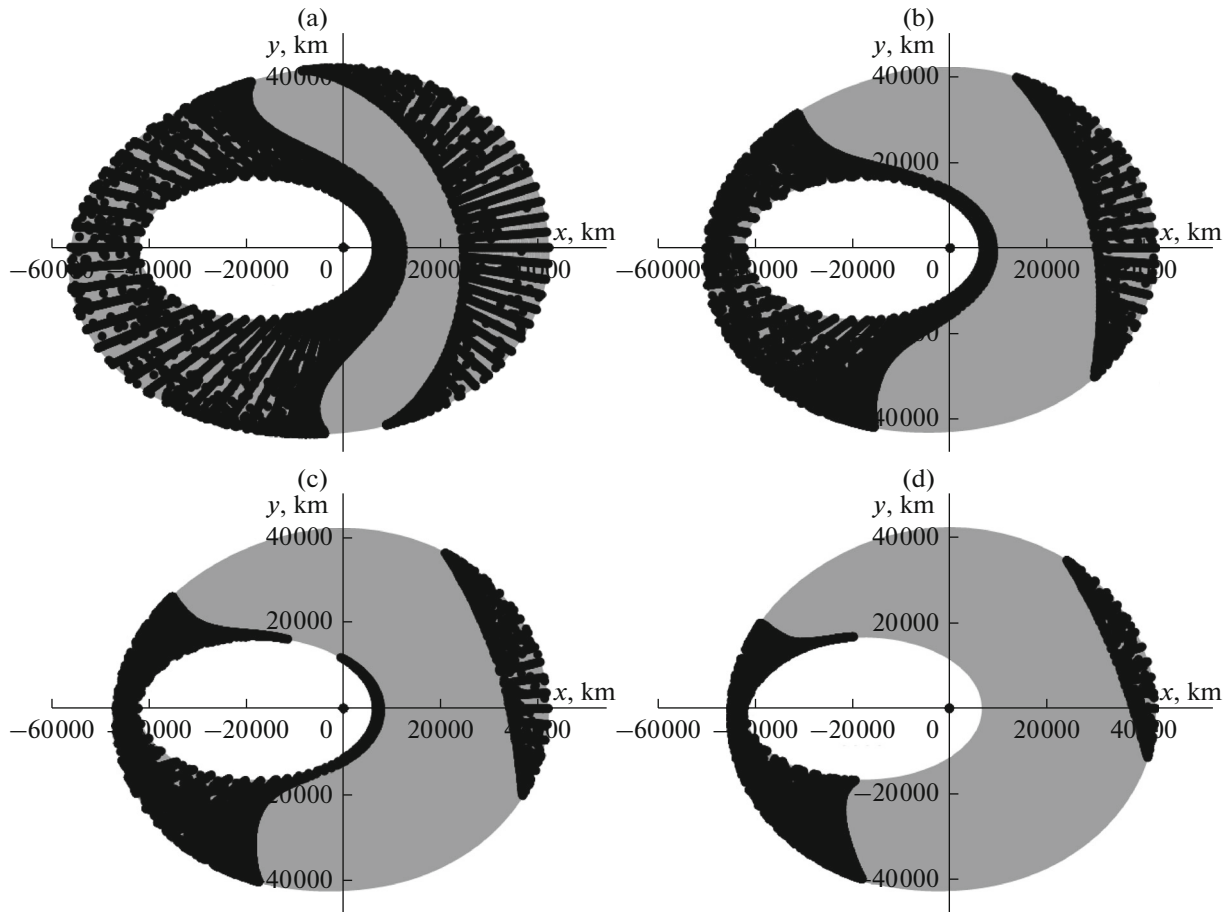
**Fig. 9.** Projection of the perturbed optimal trajectory with (a) 200, (b) 250, (c) 300, and (d) 350 revolutions onto the equatorial plane taking into account perturbations from the geopotential to the fourth degree and fourth order and the lunisolar gravity.
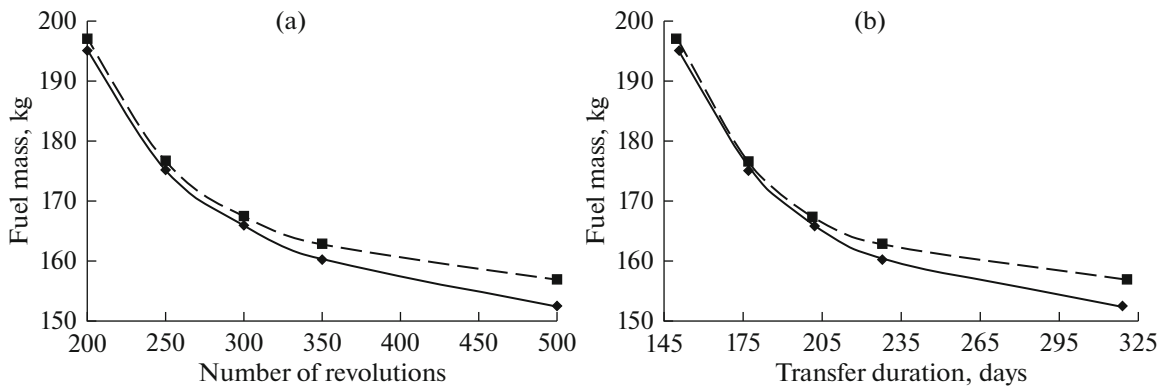


**Fig. 10.** Dependences of fuel consumption $m_p$ on the number of revolutions (left) and on transfer duration $\Delta t$ (right) for the unperturbed (solid line) and perturbed (dashed line) optimal trajectories.

lunisolar gravity. Segments of the trajectory with operating EPS are indicated by marks, and coasting segments by solid gray lines. Perturbing accelerations lead to a significant rotation of the line of apsides and line of nodes. An increase in the number of revolutions leads to an increase in the rotation of the line of apsi-

des and line of nodes during the transfer, which affects the optimal control, causing a shift in the times of switching the engines on and off and change in the pitch and yaw programs. However, the effect of the perturbing accelerations on the transfer duration and the required consumption of the fuel turned out to be

**Table 4.** Optimization results for multi-revolution transfer trajectories in the vicinity of a LEO obtained in [7] taking into account perturbations from the second zonal harmonic of the geopotential

|  | $\Delta t$, days | $N_{rev}$ | $m_p$, kg | $V_x$, m/s | $T_m$, h |
|---|---|---|---|---|---|
| Averaged problem | 5 | 63.012 | 0.8009 | 11.786 | 3.273 |
| Nonaveraged problem | 5 | 63.007 | 0.8036 | 11.826 | 3.284 |

insignificant. Figure 10 shows the dependence of fuel consumption $m_p$ on transfer duration $\Delta t$ and on the number of revolutions for the unperturbed (solid line) and perturbed (dashed line) optimal trajectories obtained in this study. It can be seen from the figure that, in this case, the perturbing accelerations lead to an increase in the fuel consumption by 1.417−4.404 kg and a decrease in the optimal transfer duration (by 0.554−1.024 days), with the exception of the transfer with an angular distance of 500 revolutions, on which the optimal duration of the perturbed trajectory exceeds the optimal duration of the unperturbed trajectory by 2.176 days. It is obvious that the action of perturbing accelerations in different problems can lead both to an increase and a decrease in the required fuel consumption and transfer duration.

## 3. OPTIMIZATION OF THE TRANSFER TRAJECTORY BETWEEN NEAR-CIRCULAR LOW EARTH ORBITS

Study [7] considered the problem of optimizing a transfer from an initial low Earth orbit (LEO) with a semimajor axis of 7792 km, eccentricity of 0.000138, inclination of 51.99°, zero argument of perigee, and right ascension of the ascending node of 256.65° to the final LEO with the same semimajor axis, eccentricity of 0.0002, inclination of 52°, argument of perigee of 11.070°, and right ascension of the ascending node of 241.57°. The initial value of the true anomaly was taken equal to 45°; the initial date of the transfer was May 9, 2021, 12:00:00 UTC; the initial spacecraft mass was 1000 kg; the thrust was 1 N; the specific impulse was 1500 s; and the number of revolutions was 63.007.

In [7], the problem under consideration was solved using the T_3D software, which includes indirect optimization methods based on the maximum principle. The solutions in [7] are presented for the averaged and nonaveraged problems taking into account the

perturbation from $J_2$. The problem was formulated using trajectory optimization with a fixed transfer duration (5 days) and free angular distance.

The problem under consideration is quite interesting in that, owing to the perturbation from the non-spherical Earth's gravitational field, an optimal solution was obtained with the correction of the right ascension of the ascending node by controlling the precession rate of the line of nodes during the transfer; therefore, the solution of this problem without taking into account the perturbations from the nonspherical Earth's gravitational field is not possible. Let us compare the results obtained using the T_3D software [7] with the results obtained using the method presented in our study [1].

Table 4 shows the results of optimization of averaged and nonaveraged trajectories from [7] (the notation is as follows: $\Delta t$ is the given transfer duration, $N_{rev}$ is the optimal angular distance of the transfer in true longitude, $m_p$ is the fuel consumption, $V_x$ is the characteristic velocity of the transfer, and $T_m$ is the burn time). Table 5 shows the results of optimization of trajectories depending on the set of perturbations obtained by the method developed in this study (here, $N_{rev}$ is a given number of revolutions and $\Delta t$ is the optimal transfer duration).

It can be seen that, for the optimal trajectory obtained in our study, taking into account perturbations only from the second zonal harmonic at a given angular distance of 63.007 revolutions, the transfer duration decreases by 220 s (0.05%) and fuel consumption decreases by 0.118 kg (~15%). This difference is probably related to the fulfillment of the necessary optimality conditions for the transfer duration in the optimization of the trajectories using the method presented in [1].

It can be seen from Table 5 that the optimal trajectories that take into account the perturbations from the terms of the expansion of the geopotential to the fourth degree and fourth order require less fuel consumption and transfer time than the trajectories that take into account perturbations from the second zonal harmonic only. The effect of perturbations from the lunisolar gravity on the transfer duration and the required fuel consumption turned out to be insignificant.

The time dependences of the orbital elements (semimajor axis, eccentricity, and right ascension of the ascending node), pitch angle, yaw angle, switching

**Table 5.** Optimization results for multi-revolution transfer trajectories in the vicinity of LEO obtained by the method developed in this study

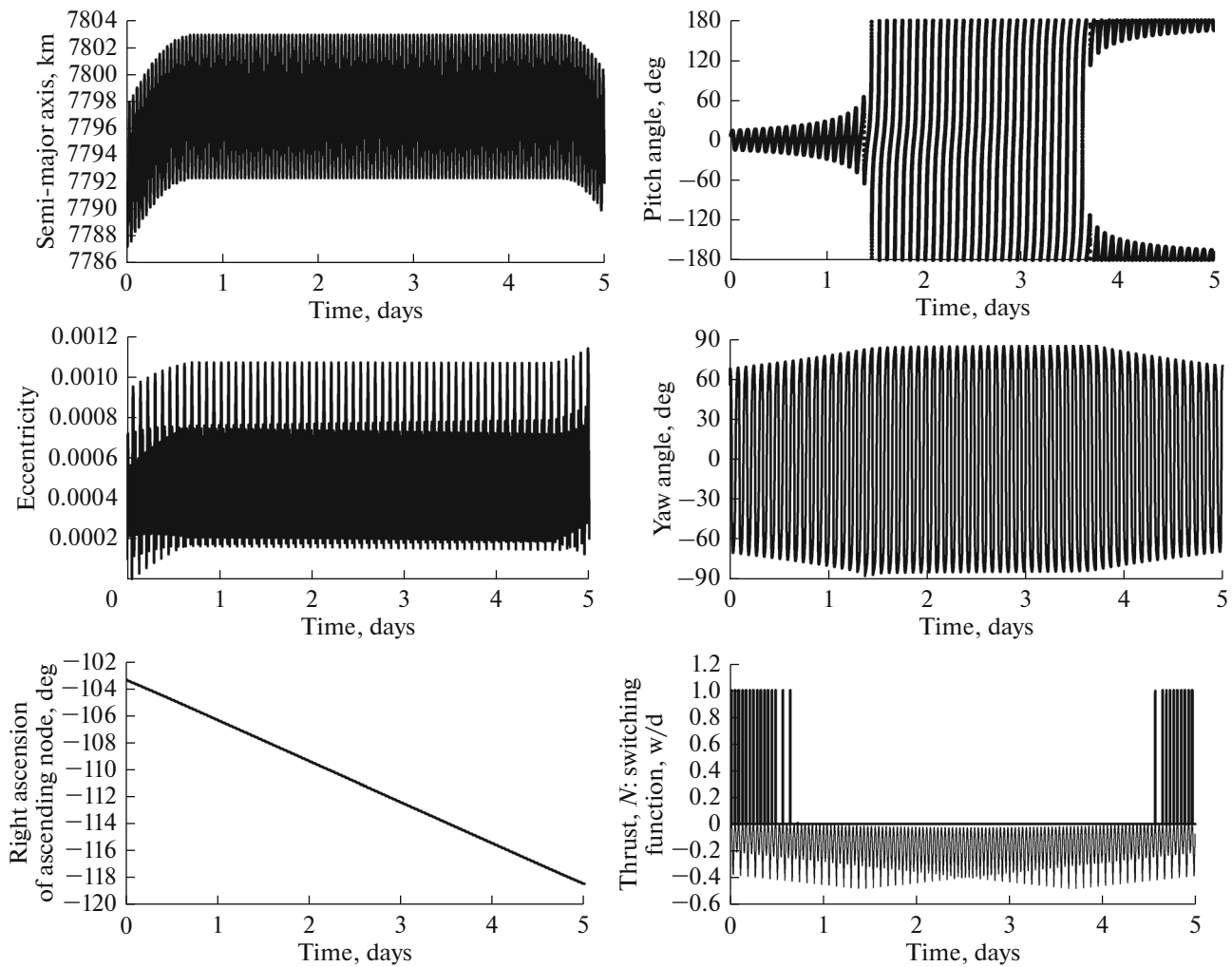| Perturbations | $N_{rev}$ | $\Delta t$, days | $m_p$, kg | $V_x$, m/s | $T_m$, h |
|---|---|---|---|---|---|
| Second zonal harmonic of the geopotential | 63.007 | 4.997454 | 0.6849 | 10.078 | 2.798 |
| Geopotential 4 × 4 | 63.007 | 4.997276 | 0.6553 | 9.643 | 2.678 |
| Geopotential 4 × 4, Moon and Sun | 63.007 | 4.997285 | 0.6565 | 9.661 | 2.683 |

**Fig. 11.** Time dependences of the semimajor axis, eccentricity, right ascension of the ascending node, pitch angle, yaw angle, switching function $S$, and thrust function $\delta$ for optimal perturbed trajectories taking into account perturbations from the second zonal harmonic.

function $S$, and thrust function $\delta$ obtained in this study for optimal perturbed trajectories taking into account perturbations from the second zonal harmonic are shown in Fig. 11.

Figure 12 shows the time dependences of the orbital elements (semimajor axis, eccentricity, and right ascension of the ascending node), pitch angle, yaw angle, switching function $S$, and thrust function $\delta$ for optimal perturbed trajectories taking into account perturbations from the terms of the expansion of geopotential up to the fourth degree and fourth order.

The right ascension of the ascending node decreases monotonically on all the trajectories, while the average value of the semimajor axis increases at the initial stage of the transfer, then remains constant for a certain time interval (waiting stage), and decreases to the initial value at the final stage of the transfer. The range of short-period oscillations of the semimajor axis at the waiting stage is 7792−7802 km, and the average

value of the semimajor axis at this stage is approximately 7797 km. In [7], the range of short-period oscillations of the semimajor axis is 7795−7805 km (the average value is 7798.5 km). The difference in the average values of the semimajor axis corresponds to the difference in the transfer duration for the trajectories obtained in [1, 7] taking into account the need to correct the right ascension of the ascending node at the waiting stage due to the difference in the precession rate of the ascending node in the initial orbit and the waiting orbit.

In the solutions obtained in [7], the EPS is switched on at the initial and final segments of the trajectory with a duration of approximately 0.5 days. In our results, the duration of the initial and final segments of the trajectory on which the EPS is switched on increases to 0.65 days, but the total duration of the EPS operation is less than in [7].
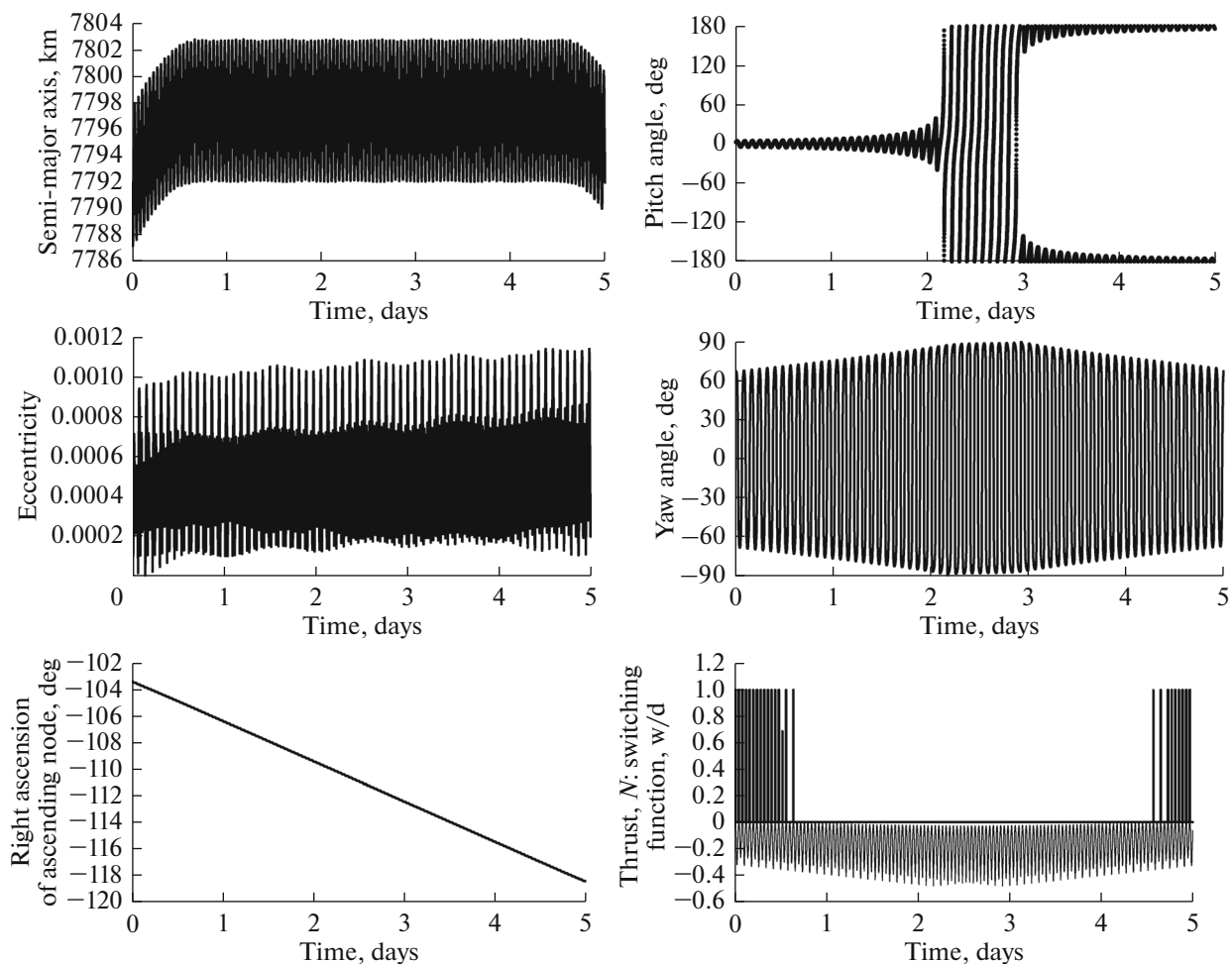
**Fig. 12.** Time dependences of the semimajor axis, eccentricity, right ascension of the ascending node, pitch angle, yaw angle, switching function $S$, and thrust function $\delta$ for optimal perturbed trajectories taking into account perturbations from the expansion terms of the geopotential up to the fourth degree and the fourth order.

Taking into account the $4 \times 4$ geopotential matrix leads to a noticeable change in the optimal pitch and yaw programs as compared to trajectories in which only the second zonal harmonic is taken into account. In particular, the length of the segment where the pitch angle changes from $-180°$ to $180°$ and the yaw angle changes from $-90°$ to $90°$ are significantly reduced.

## CONCLUSIONS

The article presents the results of applying a new method for optimizing of perturbed finite-thrust spacecraft trajectories [1]. The possibility of using the developed method to optimize the perturbed trajectories of a spacecraft with an EPS with an angular distance up to 500 revolutions is shown by the example of optimization of transfer trajectories between high elliptical orbits, geostationary transfer and geostationary orbits, and low Earth orbits. The obtained optimal perturbed trajectories are compared with the results of optimization of perturbed trajectories by other authors, and these results are shown to be close. It is shown that the formulation of the trajectory optimization problem with a fixed angular distance and free transfer duration used in [1] ensures the computational stability of the numerical method and improves the solution quality indicators by fulfilling the necessary conditions for optimality in transfer duration. The use of the algebra of complex dual numbers to calculate the required second derivatives of the perturbing accelerations allowed us to significantly simplify the preparation of a mathematical model of the optimal spacecraft motion and obtain optimal trajectories taking into account a more complicated set of perturbing accelerations than in the examples using indirect optimization methods known in the literature.

## REFERENCES

1. Petukhov, V.G. and Sung Wook Yoon, Optimization of perturbed spacecraft trajectories using complex dual numbers. Part 1: Theory and method, *Cosmic Res.,* vol. 59, no. 5, pp. 401−413.

2. Lemoine, F.G., et al. The development of the joint NASA GSFC and National Imagery and Mapping Agency (NIMA) geopotential model EGM96, *Technical Paper NASA/TP-1998-206861,* Washington, DC: Natl. Aeronaut. Space Admin., 1998.

3. Standish, E.M., JPL Planetary and Lunar Ephemerides, DE405/LE405, *JPL Interoffice Memorandum, IOM 312, F-98-048,* Pasadena, CA: Jet Propulsion Lab., 1998.

4. Petropoulos, A., Tarzi, Z.B., Lantoine, G., et al., Techniques for designing many-revolution electric-propulsion trajectories, *AAS Space Flight Mechanics Meeting, Santa Fe, New Mexico,* 2014, paper AAS 14-373.

5. Olikara, Z.P., Framework for optimizing many-revolution low-thrust transfers, *Space Flight Mechanics Conference, Snowbird, Utah,* 2018, paper AAS-18-332.

6. Aziz, D., Low-Thrust Many-Revolution Trajectory Optimization, *PhD Thesis,* University of Colorado, 2018.

7. Dargent, T., Averaging technique in T_3D an integrated tool for continuous thrust optimal control in orbit transfers, *Space Flight Mechanics Conference, Santa Fe, New Mexico,* 2014, paper AAS-14-158.

*Translated by M. Chubarova*